

Supplementary Information

Facile synthesis of 3D covalent organic frameworks via a two-in-one strategy

Xiaoli Yan,[†] Hui Li,[‡] Pengna Shang,[†] Huan Liu,[†] Jingjuan Liu,[†] Ting Zhang,[†] Guolong Xing,^{*,†} Qianrong Fang,[‡] Long Chen^{*,†}

[†]Department of Chemistry and Tianjin Key Laboratory of Molecular Optoelectronic Science, Tianjin University, Tianjin 300072, China

[‡]State Key Laboratory of Inorganic Synthesis and Preparative Chemistry, Jilin University, Changchun 130012, China

Supporting Information Placeholder

E-mail: xinggl@tju.edu.cn; Long.chen@tju.edu.cn

Contents

Section 1. Materials and Methods

Section 2. Synthetic Procedures

Section 3. NMR and Mass Spectra

Section 4. FT-IR Spectra

Section 5. PXRD Patterns

Section 6. BET Plots of N₂ Isotherms

Section 7. SEM & TEM Images

Section 8. TGA Curve

Section 9. Chemical Stability

Section 10. Acidichromic Sensor of 3D-Flu-COF

Section 11. Unit Cell Parameters and Fractional Atomic Coordinates

Section 12. Supporting References

Section 1. Materials and Methods

Materials

All the commercial available chemicals were directly used as received without further purification. 4-formylphenylboronic acid, KOH, KMnO₄, aniline hydrochloride, aniline, PdCl₂(dppf) and K₂CO₃ were purchased from Adamas. All organic solvents like *n*-butyl alcohol (*n*-BuOH), ethanol (EtOH), mesitylene, tetrahydrofuran (THF), acetone, dimethylacetamide (DMAc), dichloromethane (DCM), benzyl alcohol and dioxane were analytical grade and used without further purification. 4,4'-(3,6-bis(4-(5,5-dimethyl-1,3-dioxan-2-yl)phenyl)-9H-fluorene-9,9-diyl)dianiline (A₂B₂-Flu) was unambiguously characterized by NMR, MALDI-TOF MS.

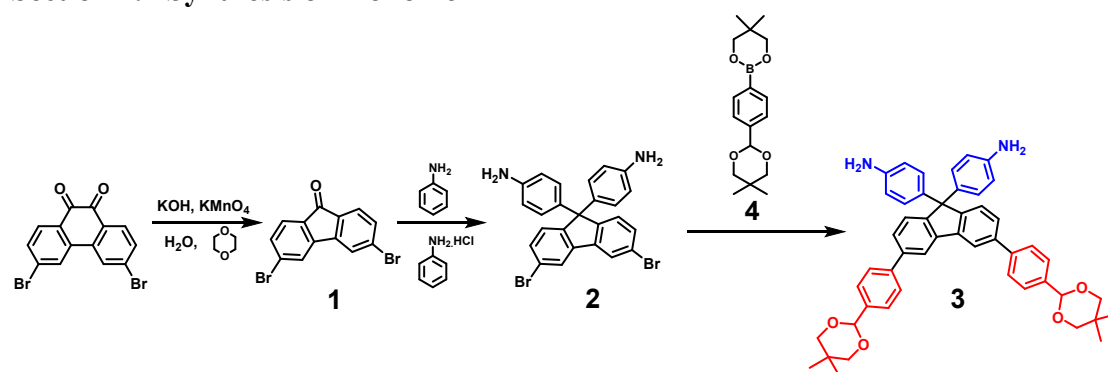
Physical measurements

¹H and ¹³C NMR spectra of all monomers were carried out on a Bruker AVANCE III-400MHz NMR spectrometer. The Powder X-ray diffraction (PXRD) patterns were recorded on X-ray diffractometer (RIGAKU SMARTLAB 9KW) with a Cu-target tube and a graphite monochromator. Surface areas were measured by nitrogen adsorption and desorption at 77 K using a Bel Japan Inc. model BELSOPR-max analyzer and the samples were degassed at 150 °C for 8 h under vacuum (10⁻⁵ bar) before analysis. The pore size distribution was calculated from the adsorption branch using the nonlocal density functional theory (NLDFT). Fourier transform infrared (FT-IR) spectra were recorded in transmission mode on a Bruker Alpha spectrometer using KBr pellets in the range 400–4000 cm⁻¹. The UV-vis absorption spectra were obtained from PerkinElmer Lambda 750 spectrophotometer equipped with integration sphere. The ¹³C cross-polarization magic angle spinning (CP/MAS) spectra were recorded on Varian Infinityplus 300 (300 MHz) solid state NMR spectrometer with a 4 mm double resonance MAS probe and at a MAS rate of 10.0 kHz with a contact time of 2 ms (ramp 100) and a pulse delay of 3 s. High-resolution mass spectrum was obtained with a Micro mass GCT-TOF mass spectrometer. The mass spectrum was recorded by matrix-assisted laser desorption ionization time-of-

flight (MALDI-TOF) mass spectroscopy with Bruker Autoflex speed TOF mass spectrometer. The thermogravimetric analysis (TGA) of 3D-Flu-COF was evaluated with a differential thermal analysis instrument (TA Instruments TGA Q50-1918 analyzer) over the temperature range from 20 to 800 °C under N₂ atmosphere at a heating rate of 10 °C min⁻¹ using an empty Al₂O₃ crucible as the reference. Transmission electron microscopies (TEM) were performed on a FEI model Tecani 20 microscope or a JEOL model JEM-2100F. Field emission scanning electron microscopies (FE-SEM) were carried out using a Hitachi Limited model SU8010 microscope operating at an accelerating voltage of 5.0 kV. Elemental analysis (C, H, N) was performed on a Perkin-Elmer 240C elemental analyzer. The simulations of the possible structures were carried out in Accelrys Material Studio 8.0 software package. The simulated PXRD patterns were obtained by the Reflex module. Pawley refinement of the experimental PXRD of 3D-Flu-COF was conducted to optimize the lattice parameters iteratively until the R_{wp} value converges.

Section 2. Synthetic Procedures

Section 2.1 Synthesis of Monomer



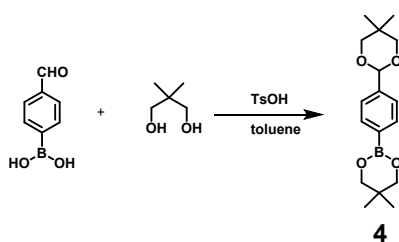
Scheme S1. Synthetic routes of 4,4'-(3,6-bis(4-(5,5-dimethyl-1,3-dioxan-2-yl)phenyl)-9H-fluorene-9,9-diyl)dianiline (**3**).

3,6-dibromofluorenone (1): This compound was prepared according to the reported procedures.^[S1]

4,4'-(3,6-dibromo-9H-fluorene-9,9-diyl)dianiline (2): A mixture of 3,6-dibromofluorenone (**1**) (159 mg, 0.47 mmol), aniline hydrochloride (172 mg, 1.33

mmol), aniline (2 mL, 21.47 mmol) were heated at 135 °C for 24 h. After cooling to room temperature, 2 mL 10 % NaOH aqueous solution was added to the reaction mixture, and was stirred for 0.5 h. The crude product was collected by extraction with ethyl acetate for three times. The organic solvent was evaporated under vacuum and the residue was purified by recrystallization using ethyl ether to afford **2** as a white solid (109 mg, 46%). ¹H NMR (400 MHz, DMSO-*d*₆) δ 8.23 (s, 2H), 7.47 (d, *J* = 6.7 Hz, 2H), 7.29 (d, *J* = 8.2 Hz, 2H), 6.73 (d, *J* = 8.4 Hz, 4H), 6.42 (d, *J* = 8.4 Hz, 4H), 5.01 (s, 4H). ¹³C NMR (100 MHz, DMSO-*d*₆) δ 152.22, 147.86, 140.91, 131.84, 131.24, 128.55, 128.34, 124.36, 120.96, 114.12, 63.70. GCT-TOF: *m/z* (C₂₅H₁₈Br₂N₂) calculated for [M + H⁺] 506.24, found, 506.99.

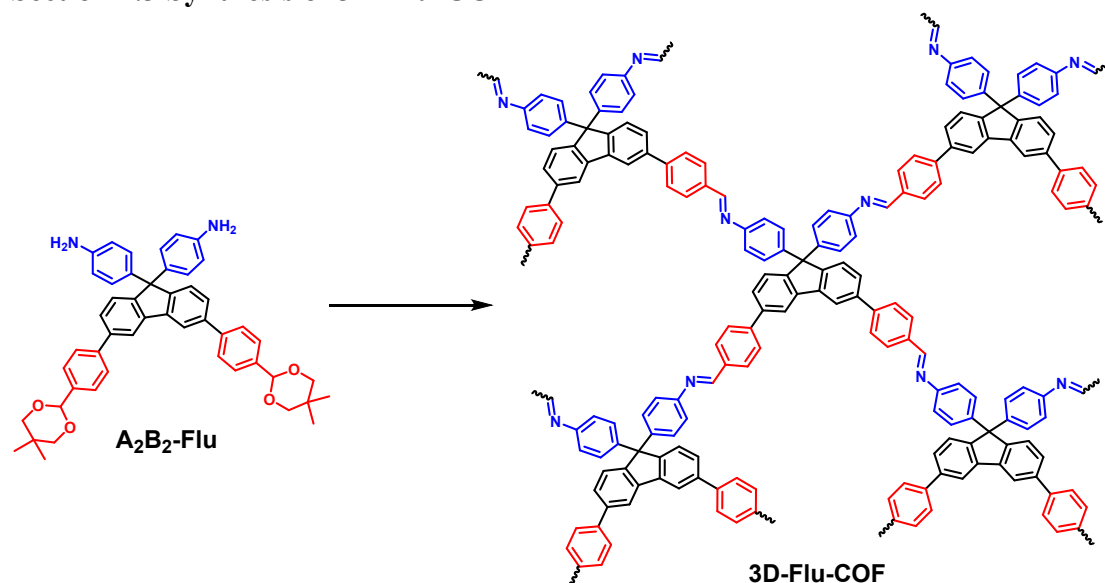
4,4'-(3,6-bis(4-(5,5-dimethyl-1,3-dioxan-2-yl)phenyl)-9H-fluorene-9,9-diyl)dianiline (3): 2-(4-(5,5-dimethyl-1,3-dioxan-2-yl)phenyl)-5,5-dimethyl-1,3,2-dioxaborinane (**4**) (119 mg, 0.39 mmol), PdCl₂(dppf) (15 mg, 0.02 mmol), and compound **2** (86 mg, 0.17 mmol) were dissolved in dioxane (4 mL). Then, 0.4 mL of aqueous K₂CO₃ (2.6 M, 145 mg, 1.05 mmol) was added. After degassing by argon bubbling, the reaction mixture was heated to 100 °C for 24 h. After cooling to room temperature, the mixture was diluted with water and extracted with ethyl acetate. The combined organic phase was washed with water and dried over anhydrous MgSO₄. The solvent was evaporated under vacuum and the residue was purified by column chromatography on silica gel (petroleum ether/ethyl acetate = 5/1) to give **3** as a white solid (65 mg, 53%). ¹H NMR (400 MHz, DMSO-*d*₆) δ 8.37 (s, 2H), 7.81 (d, *J* = 7.8 Hz, 4H), 7.61 (d, *J* = 7.9 Hz, 2H), 7.54 (d, *J* = 7.8 Hz, 4H), 7.42 (d, *J* = 7.9 Hz, 2H), 6.83 (d, *J* = 8.1 Hz, 4H), 6.44 (d, *J* = 8.1 Hz, 4H), 5.48 (s, 2H), 4.97 (s, 4H), 3.68 (q, *J* = 10.8 Hz, 8H), 1.21 (s, 6H), 0.77 (s, 6H). ¹³C NMR (100 MHz, DMSO-*d*₆) δ 152.48, 147.60, 140.89, 140.48, 139.16, 138.28, 133.08, 128.71, 127.17, 126.89, 126.73, 119.28, 114.10, 101.06, 77.05, 63.75, 23.24, 21.90. GCT-TOF: *m/z* (C₄₉H₄₈N₂O₄) calculated for [M + H⁺] 729.36, found, 729.37.



Scheme S2. Synthetic routes of 2-(4-(5,5-dimethyl-1,3-dioxan-2-yl)phenyl)-5,5-dimethyl-1,3,2-dioxaborinane (**4**):

2-(4-(5,5-dimethyl-1,3-dioxan-2-yl)phenyl)-5,5-dimethyl-1,3,2-dioxaborinane (4**):** 4-formylphenylboronic acid (3.0 g, 20 mmol), neopentyl glycol (4.56 g, 44 mmol) and *p*-toluenesulfonic acid (69 mg, 0.0004 mmol) were dissolved in toluene (30 mL). After degassing by argon bubbling, the reaction mixture was heated at 115 °C overnight. After cooling to room temperature, dichloromethane was add and the reaction mixture was washed with saturated sodium bicarbonate solution. The combined organic phase was dried over anhydrous MgSO₄. The solvent was evaporated under vacuum and the residue was purified by recrystallization using ethanol to obtain **4** as a white needle-like solid (4.0 g, 67%). ¹H NMR (400 MHz, CDCl₃) δ 7.80 (d, *J* = 7.9 Hz, 2H), 7.48 (d, *J* = 7.9 Hz, 2H), 5.39 (s, 1H), 3.77 (d, *J* = 8.6 Hz, 6H), 3.65 (d, *J* = 10.9 Hz, 2H), 1.29 (s, 3H), 1.01 (s, 6H), 0.80 (s, 3H). ¹³C NMR (100 MHz, CDCl₃) δ (ppm) 140.64, 133.89, 125.26, 101.81, 72.29, 31.89, 30.29, 23.09, 21.93. MALDI-TOF mass, *m/z*: Anal. Calcd. for C₁₇H₂₅BO₄ [M-H]⁻ 303.19, found, 303.19.

Section 2.3 Synthesis of 3D-Flu-COF



Scheme S3. Synthetic routes for 3D-Flu-COFs.

3D-Flu-COF:

A 10 mL Pyrex tube was charged with A₂B₂-Flu (20 mg, 0.027 mmol), and specific organic solvent (0.5 mL) (e.g. *n*-Butanol, mesitylene, benzyl alcohol, dioxane *etc.*) was added. After the mixture was sonicated for 1 min, 0.4 mL of aqueous solution of acetic acid (6.0 M) was added. The mixture was sonicated for another 1 min and further degassed by three freeze-pump-thaw cycles, purged with N₂ and then heated at 120 °C for 7 days. A off-white precipitate was formed, which was collected by sucking filtration and sequentially washed with *N,N*-dimethylformamide, anhydrous ethanol, and tetrahydrofuran. The collected sample was dried under vacuum for 24 h to afford an off-white powder in high isolated yields: 90-97%. ¹³C CP-MAS NMR (75 MHz, solid state): δ (ppm) 159, 153, 150, 143, 140, 138, 136, 129, 127, 118, 68, 65, 30, 26, 22. Anal. Calcd. for (C₃₉H₂₄N₂)_n (theoretical formula for an infinite 3D-Flu-COF): C, 89.97; H, 4.65; N, 5.38. Found: C, 84.02; H, 5.93; N, 5.23.

Table S1. Porosity and yields of 3D-Flu-COFs synthesized from different solvents.

Solvents	Notation of 3D-Flu-COF	BET surface areas (m ² /g)	Pore size distribution (nm)	Yield (%)
Benzyl alcohol	3D-Flu-COF _{benzyl alcohol}	1590	1.15	97
<i>n</i> -BuOH	3D-Flu-COF _{<i>n</i>-BuOH}	1510	1.15	92
Dioxane	3D-Flu-COF _{dioxane}	1300	1.15	97
Mesitylene	3D-Flu-COF _{mesitylene}	1270	1.20	90

Section 3. NMR and MALDI-TOF Mass Spectra

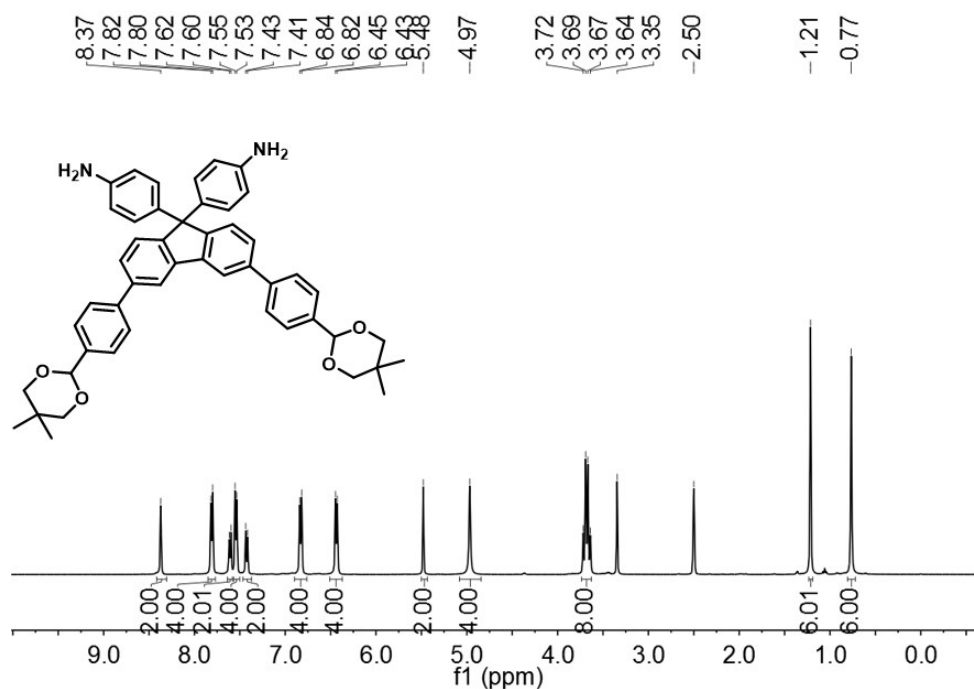


Fig. S1. ¹H NMR spectrum (400 MHz, DMSO-*d*₆) of 4,4'-(3,6-bis(4-(5,5-dimethyl-1,3-dioxan-2-yl)phenyl)-9H-fluorene-9,9-diyl)dianiline (**3**).

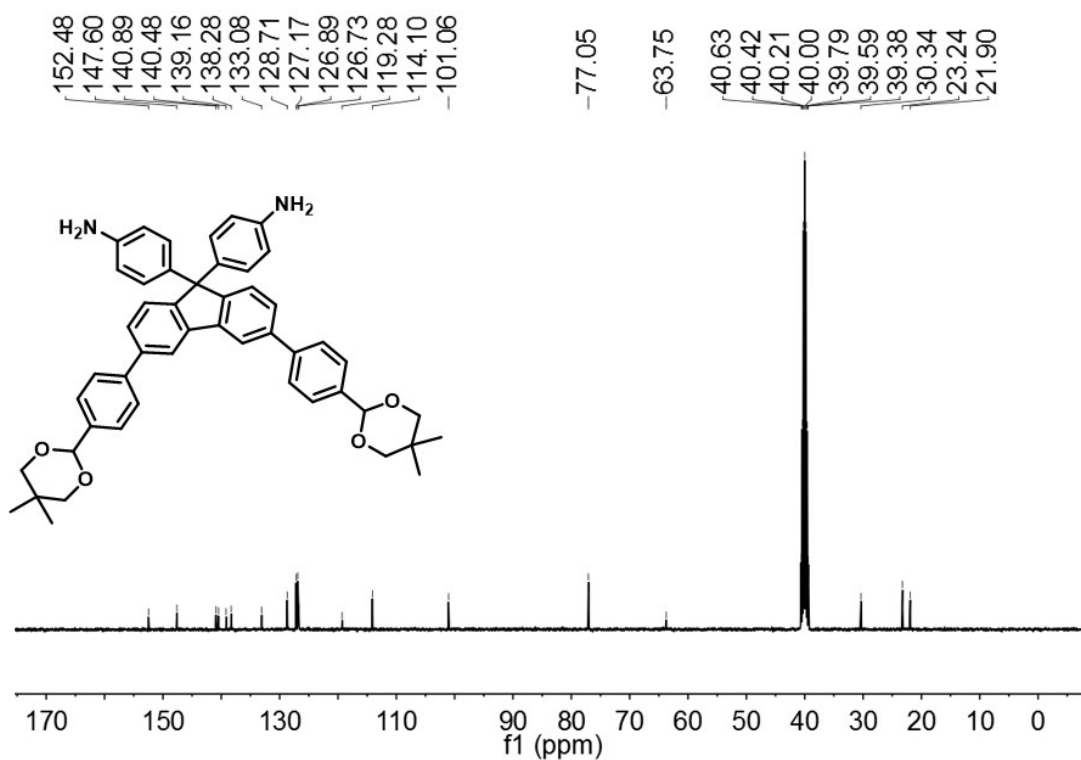


Fig. S2. ^{13}C NMR spectrum (100 MHz, $\text{DMSO-}d_6$) of 4,4'-(3,6-bis(4-(5,5-dimethyl-1,3-dioxan-2-yl)phenyl)-9H-fluorene-9,9-diyl)dianiline (**3**).

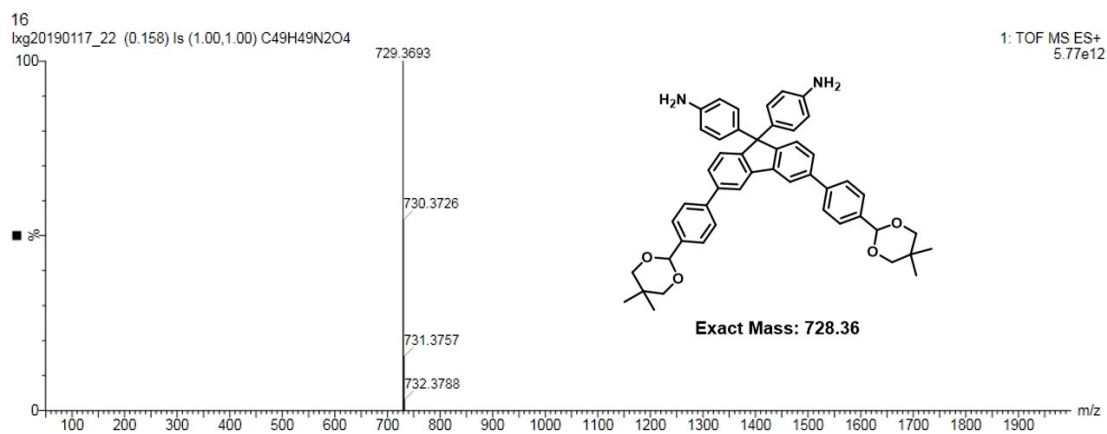


Fig. S3. The high resolution GCT-TOF mass spectrum of 4,4'-(3,6-bis(4-(5,5-dimethyl-1,3-dioxan-2-yl)phenyl)-9H-fluorene-9,9-diyl)dianiline (**3**).

Section 4. FT-IR Spectra

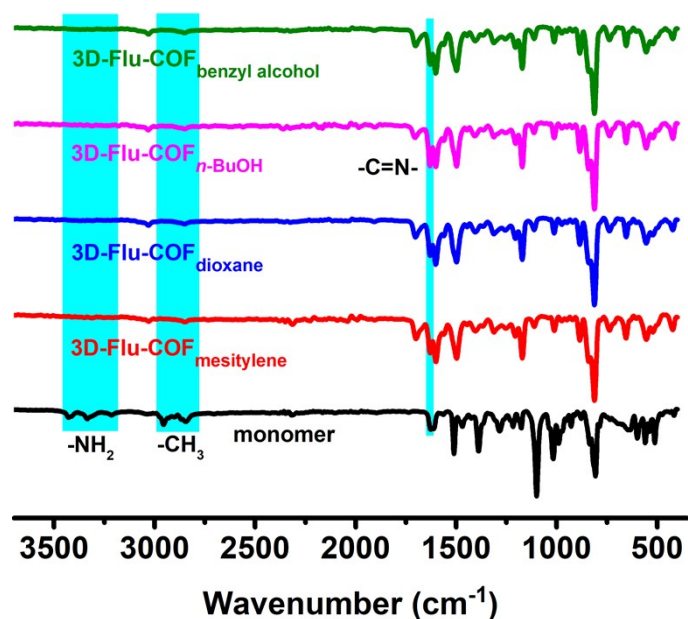


Fig. S4. FT-IR spectra of monomer (A₂B₂-Flu) (black), and 3D-Flu-COFs prepared in different solvents, 3D-Flu-COF_{benzyl alcohol} (olive), 3D-Flu-COF_{n-BuOH} (magenta), 3D-Flu-COF_{dioxane} (blue), 3D-Flu-COF_{mesitylene} (red).

Section 5. PXRD Patterns

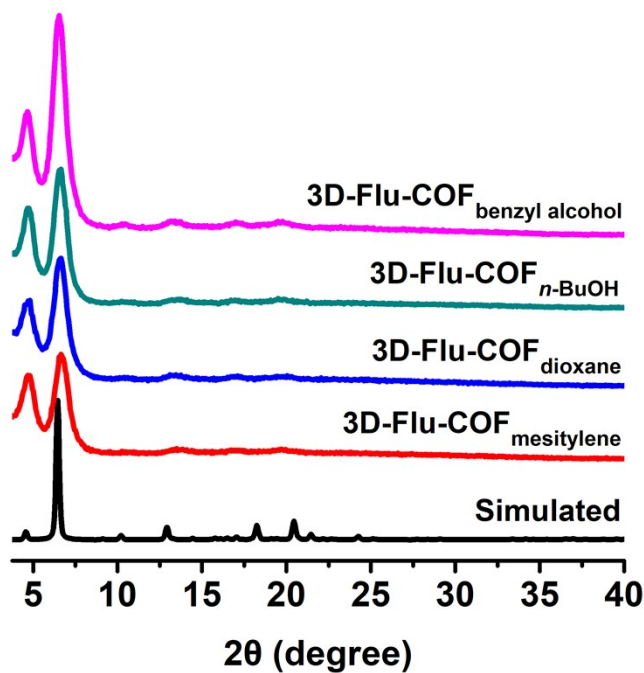


Fig. S5. PXRD patterns of 3D-Flu-COFs prepared in different solvents.

Section 6. BET Plots of N₂ Isotherms

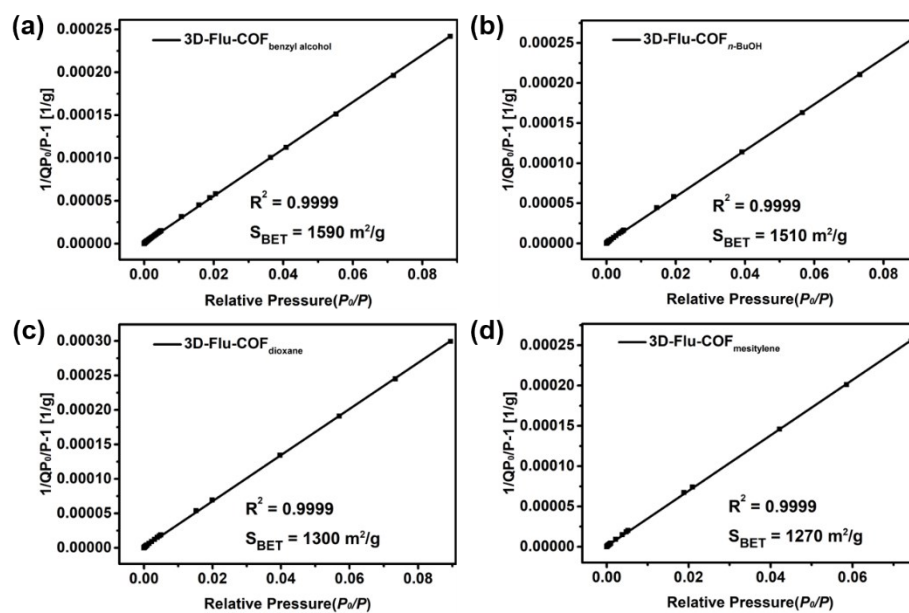


Fig. S6. BET plots of 3D-Flu-COFs prepared in different solvents. (a) 3D-Flu-COF_{benzyl alcohol}, (b) 3D-Flu-COF_{n-BuOH}, (c) 3D-Flu-COF_{dioxane}, (d) 3D-Flu-COF_{mesitylene}.

Section 7. SEM & TEM Images

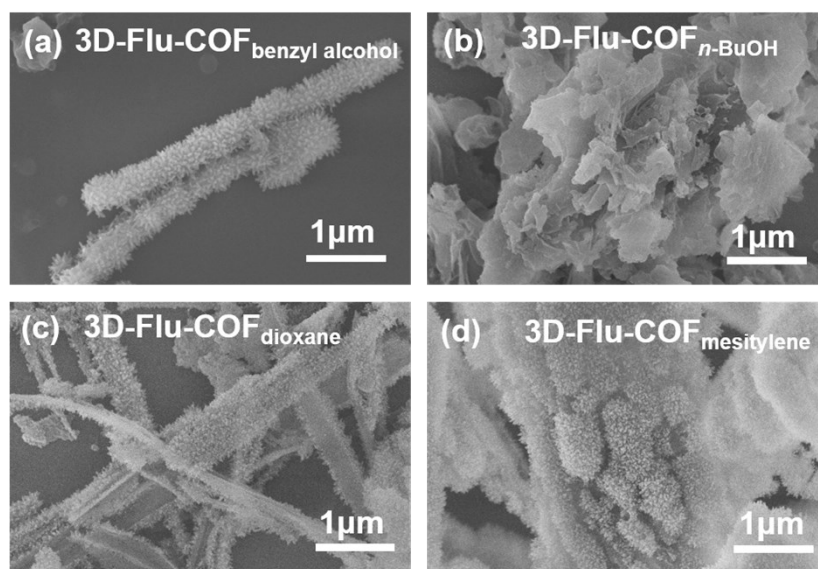


Fig. S7. SEM images of 3D-Flu-COFs synthesized in different solvents, (a) 3D-Flu-COF_{benzyl alcohol}, (b) 3D-Flu-COF_{n-BuOH}, (c) 3D-Flu-COF_{dioxane}, (d) 3D-Flu-COF_{mesitylene}.

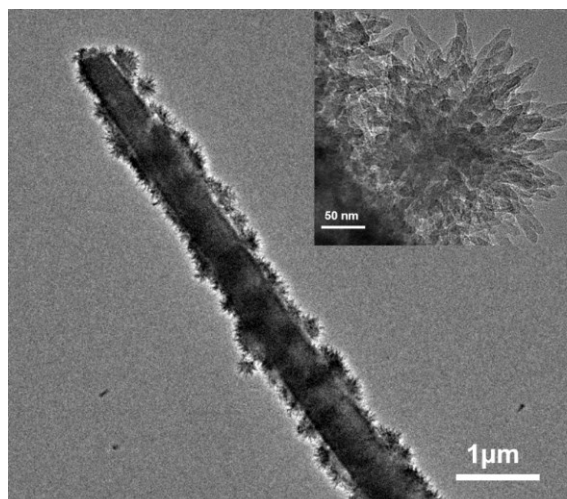


Fig. S8. TEM images of 3D-Flu-COF_{benzyl alcohol}.

Section 8. TGA Curve

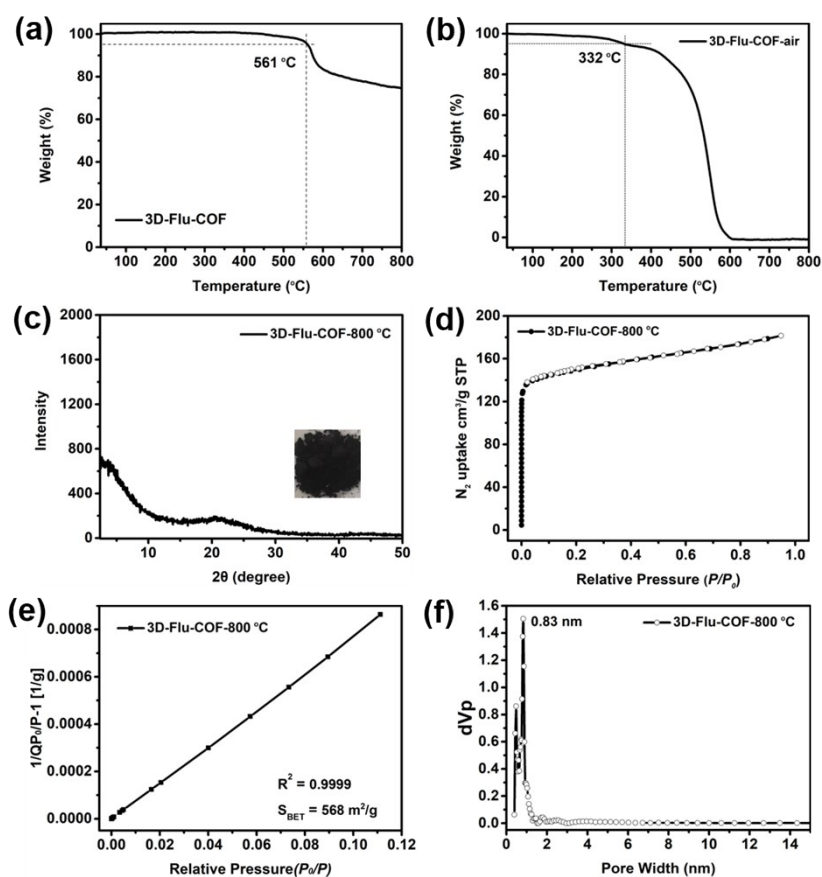
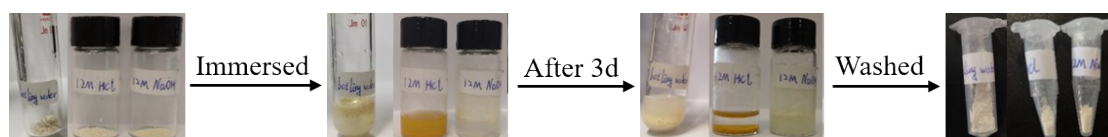


Fig. S9. (a), (b) Thermogravimetric analysis profiles of 3D-Flu-COF_{benzyl alcohol} ranging from room temperature to 800 °C at 10 °C/min under nitrogen and air atmosphere, respectively; (c) PXRD patterns (insert shows the photograph of 3D-Flu-COF-800 °C), (d) N₂ adsorption (solid symbols) and desorption (open symbols) isotherms, (e) BET plots, (f) pore size distribution profiles of 3D-Flu-COF after treatment at 800 °C for 1 hour under nitrogen atmosphere.

Section 9. Chemical Stability

The experimental procedures towards chemical stability of 3D-Flu-COF_{benzyl alcohol} powder: 20 mg of 3D-Flu-COF_{benzyl alcohol} was suspended in the corresponding solutions for 3 days, respectively. Then the sample was collected by sucking filtration and sequentially washed with saturated sodium bicarbonate solution (for sample treated with 12 M HCl) or dilute hydrochloric acid solution (for sample treated with 12 M NaOH), deionized water and anhydrous ethanol to neutral. The collected sample was dried under vacuum for 24 h.



Scheme S4. Optical photographs of 3D-Flu-COF_{benzyl alcohol} before and after treatments in boiling water, 12 M HCl, and 12 M NaOH for 3 days.

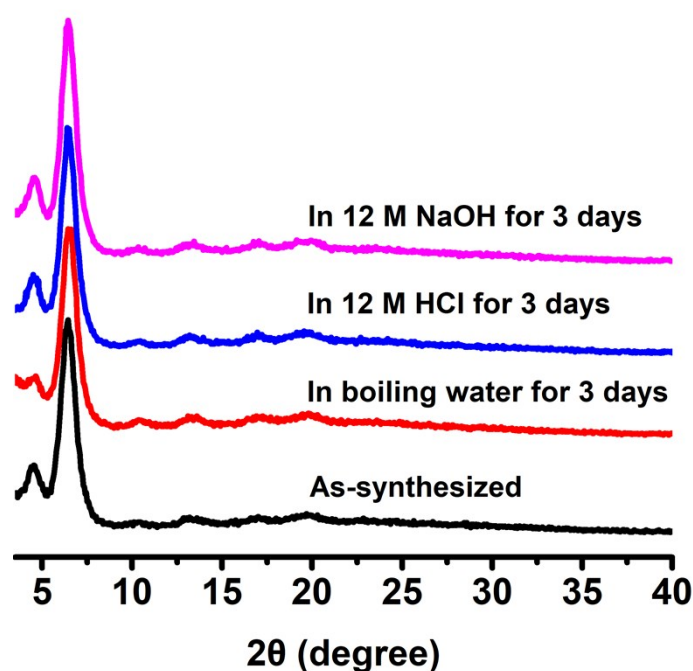


Fig. S10. PXRD patterns of 3D-Flu-COF_{benzyl alcohol} measured before (black) and after treatments in boiling water (red), 12 M HCl (blue), and 12 M NaOH (magenta) for 3 days.

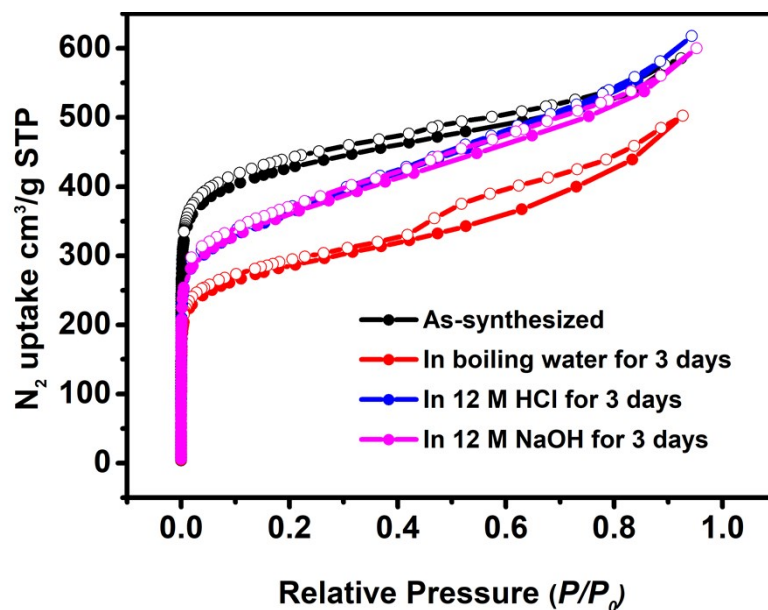


Fig. S11. N_2 adsorption (solid symbols) and desorption (open symbols) isotherms of 3D-Flu-COF_{benzyl alcohol} measured before (black) and after treatments in boiling water (red), 12 M HCl (blue), and 12 M NaOH (magenta) for 3 days.

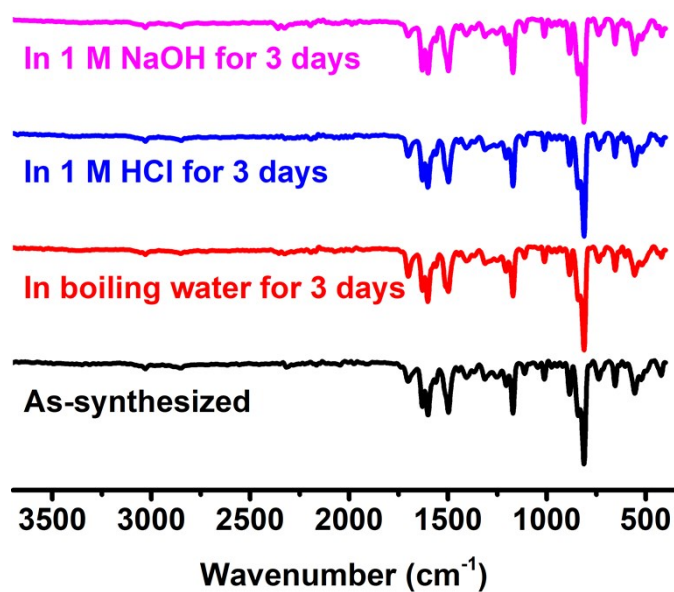


Fig. S12. FT-IR spectra of 3D-Flu-COF_{benzyl alcohol} before (black) and after treatments in 12 M NaOH (magenta), 12 M HCl (blue), and boiling water (red) for 3 days.

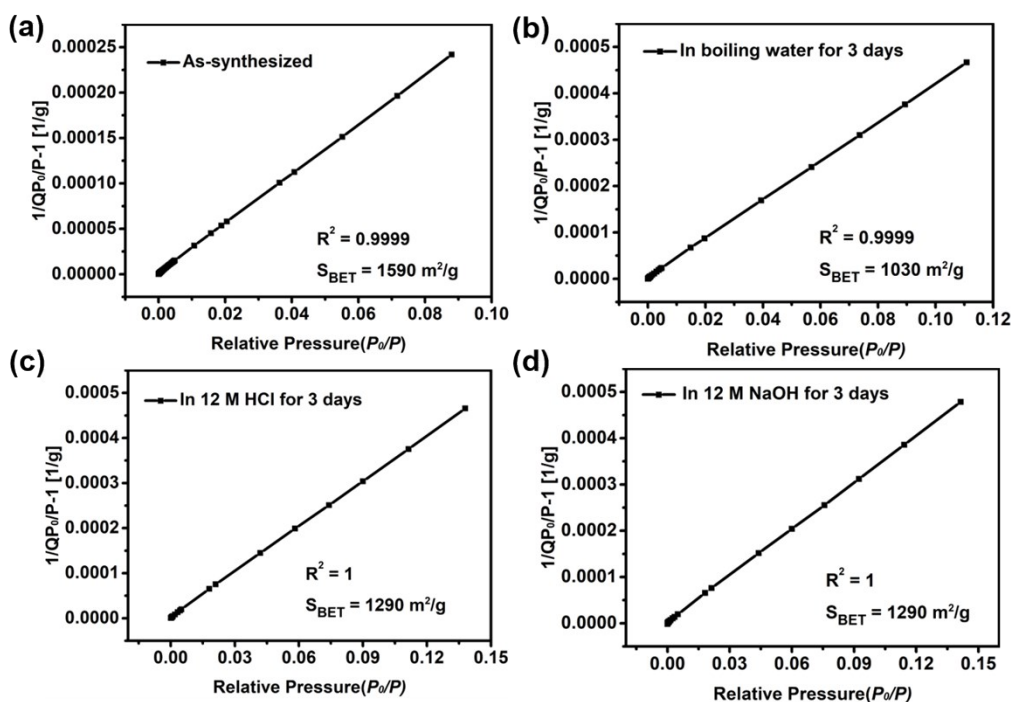


Fig. S13. BET plots of 3D-Flu-COF_{benzyl alcohol} before (a) after treatments in boiling water (b), 12 M HCl (c), and 12 M NaOH (d) for 3 days. The BET surface areas were 1590, 1030, 1290, 1290 m²/g, respectively.

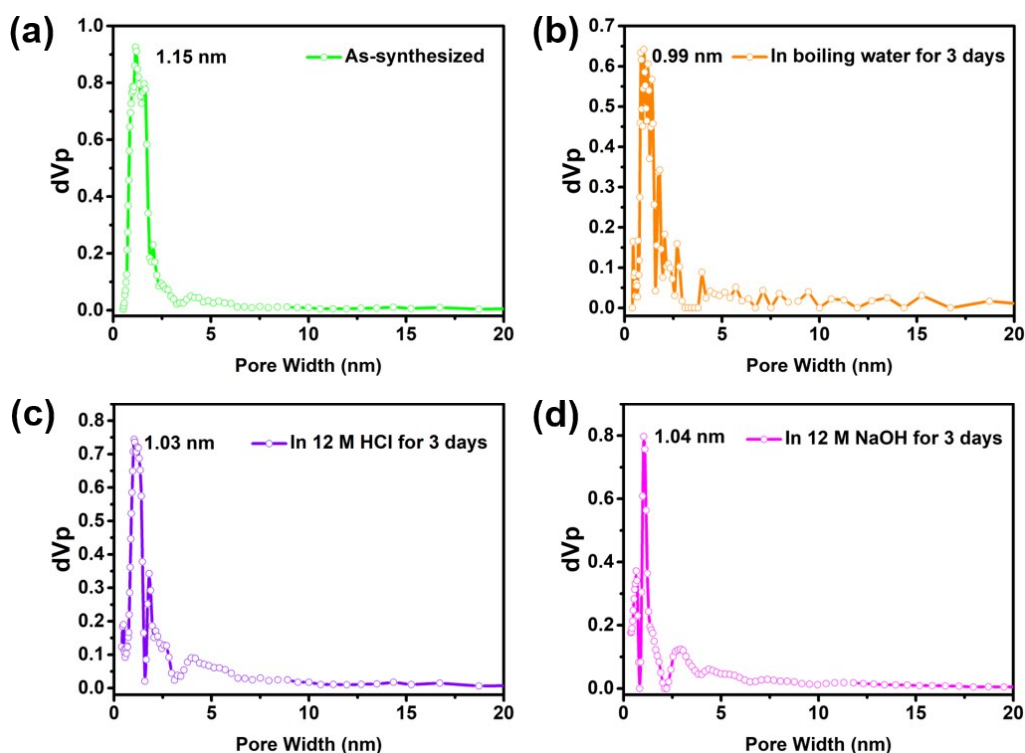


Fig. S14. Pore size distribution of 3D-Flu-COF_{benzyl alcohol} before (a) after treatments in boiling water (b), 12 M HCl (c), and 12 M NaOH (d) for 3 days.

Section 10. The Protonation and Deprotonation Process of 3D-Flu-COF

The experimental procedures of 3D-Flu-COF powder response to different TFA concentrations: 10 mg of 3D-Flu-COFbenzyl alcohol was suspended in 10 mL dioxane solution of TFA at specified concentration for 5 min. Then the acidified sample was separated from solution by vacuum filtration, and dried at room temperature for 2 min before measuring by UV-vis spectra.

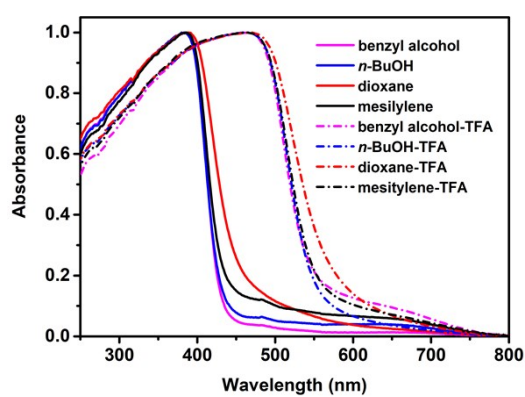


Fig. S15. UV/Vis absorption spectra of 3D-Flu-COFs powder prepared in different solvents before (solid) and after (short dash dot) treatment of TFA vapor.

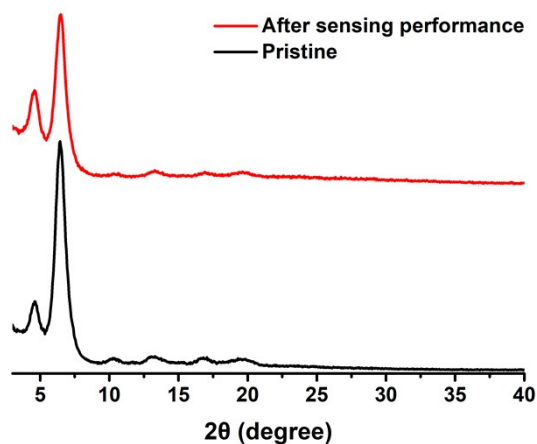


Fig. S16. PXRD patterns of 3D-Flu-COF_{benzyl alcohol} before (black) and after (red) treatment of TFA sensing performance.

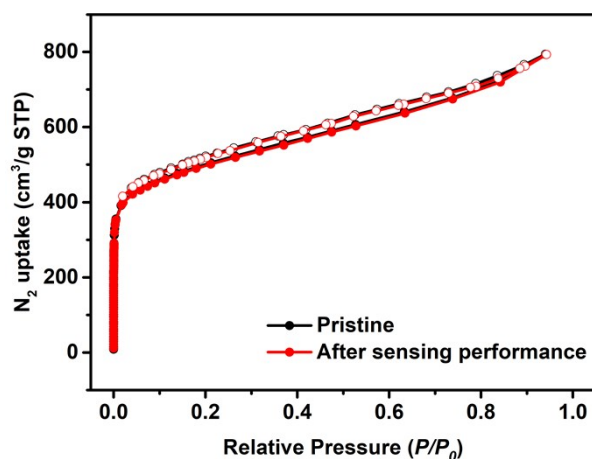


Fig. S17. N₂ adsorption/desorption isotherms of 3D-Flu-COF_{benzyl alcohol} before (black) and after (red) treatment of TFA sensing performance.

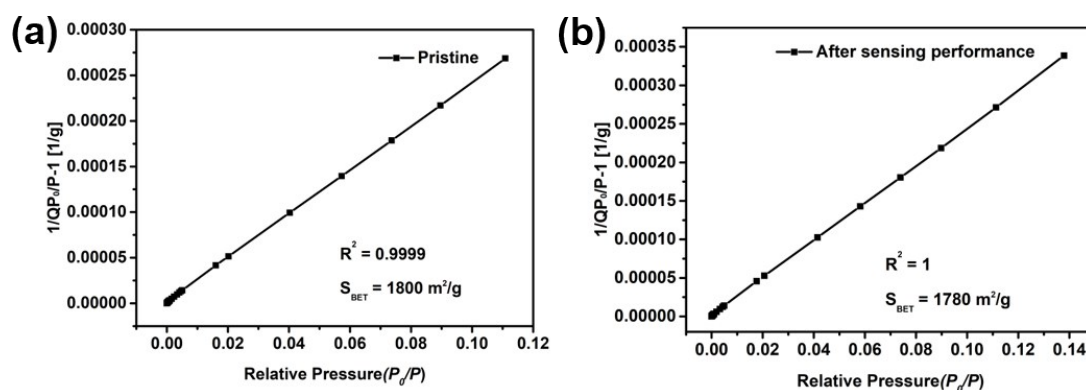


Fig. S18. BET surface area plot of 3D-Flu-COF_{benzyl alcohol} before (a) and after (b) treatment of TFA sensing performance.

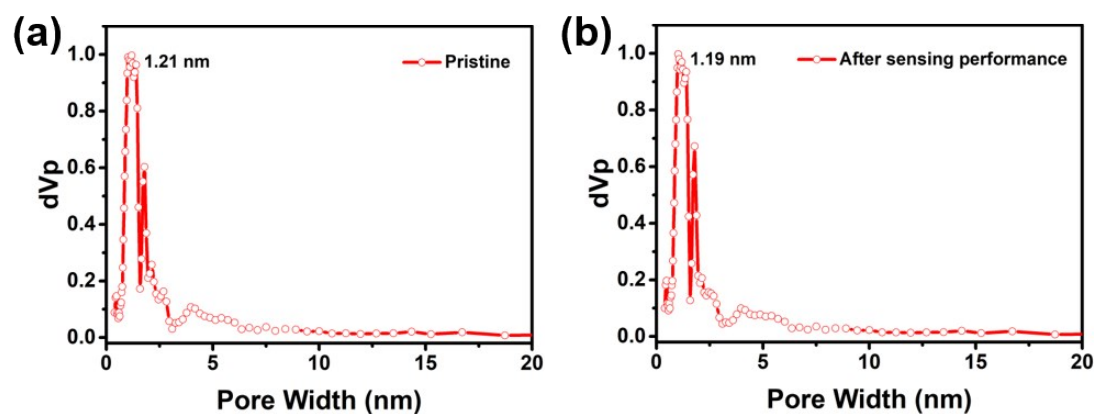


Fig. S19. Pore size distribution profiles of 3D-Flu-COF_{benzyl alcohol} before (a) and after (b) treatment of TFA sensing performance.

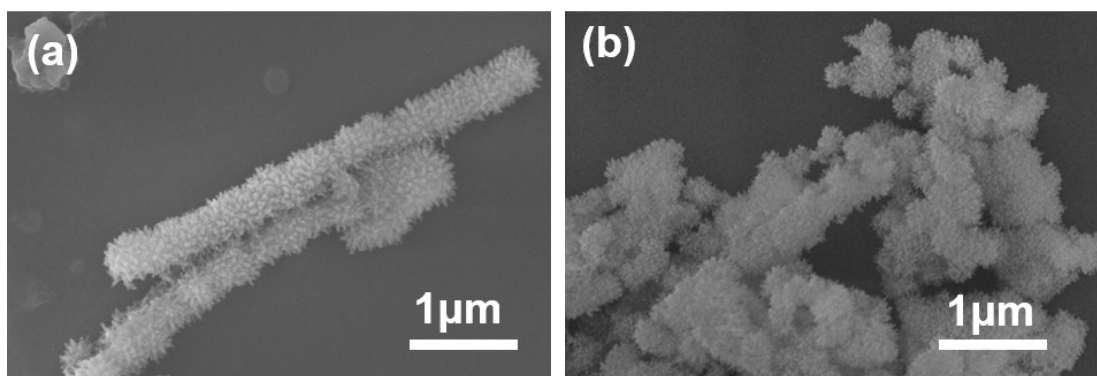


Fig. S20. SEM images of 3D-Flu-COF_{benzyl alcohol} before (a) and after (b) treatment of TFA sensing performance.

Table S2. Sensing performance comparison of this work with other COFs.

Materials	Detection limit for TFA solutions (mm L ⁻¹)	Response range for TFA solutions (orders of magnitude)	Ref.
Py-TT-COF	10	2	<i>J. Am. Chem. Soc.</i> , 2019, 141 ,
Per-N-COF	35 μg L ⁻¹ (TFA vapour)	4	15693-15699
Py-COF	0.3	2	<i>Chem. Commun.</i> , 2020, 56 ,
BCzP-COF	1	2	3253-3256
3D-Flu-COF	0.2	4	This work

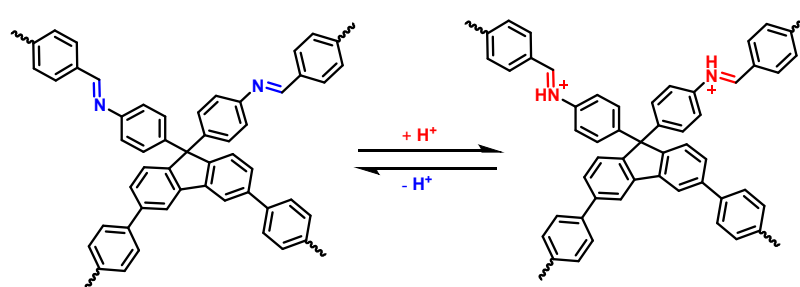


Fig. S21. Proposed protonation and deprotonation process in the framework of 3D-Flu-COF_{benzyl alcohol} upon the treatments of TFA vapor and TEA vapor.

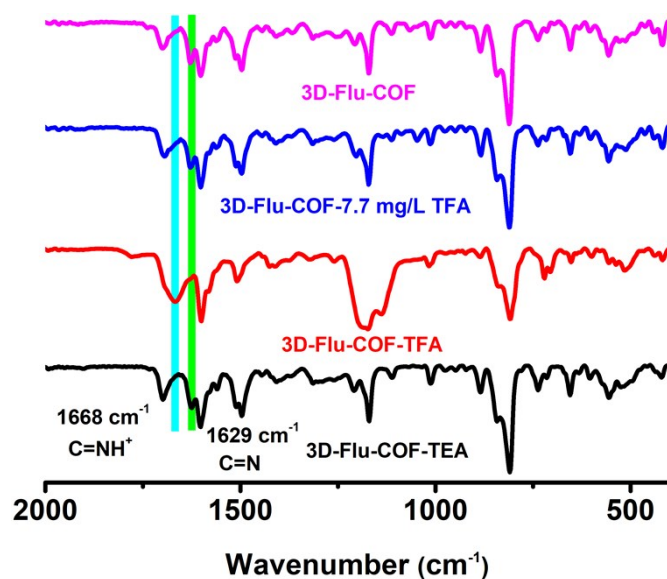


Fig. S22. FT-IR spectra of the protonated and the neutral 3D-Flu-COF_{benzyl alcohol}.

Section 11. Unit Cell Parameters and Fractional Atomic Coordinates

Table S3. Unit cell parameters and fractional atomic coordinates for 3D-Flu-COF_{benzyl alcohol} calculated based on the 7-interpenetrated **dia** net.

Space group: <i>P43</i>			
$a = b = 27.3960 \text{ \AA}$, and $c = 7.1325 \text{ \AA}$.			
$\alpha = \beta = \gamma = 90^\circ$			
	X	Y	Z
C1	0.79119	0.20592	0.97018
C2	0.77655	0.23438	1.12618
C3	0.83208	0.21783	0.85251
C4	0.86289	0.25939	0.87335
C5	0.84729	0.28971	1.03829
C6	0.8047	0.27741	1.16445
C7	0.90766	0.26627	0.71716
C8	0.91637	0.2326	0.56299
C9	0.9553	0.23635	0.41962
C10	0.98235	0.30838	0.56499

C11	0.94352	0.30461	0.70816
C12	1.17893	0.27063	-0.34743
C13	1.16782	0.30764	-0.20791
C14	1.12879	0.30495	-0.06404
C15	1.096	0.26428	-0.0405
C16	1.10697	0.2275	-0.17946
C17	1.14578	0.23029	-0.32227
N18	1.05413	0.25794	0.10695
C19	1.03612	0.28346	0.25849
C20	0.99112	0.27478	0.41137
C21	0.69669	0.77887	0.08448
C22	0.72394	0.73498	0.11766
C23	0.65428	0.79119	0.21235
C24	0.63752	0.75944	0.3718
C25	0.66677	0.71657	0.38346
C26	0.70773	0.70499	0.26611
C27	0.59281	0.76419	0.53014
C28	0.56574	0.80663	0.5953
C29	0.52779	0.80632	0.74605
C30	0.5393	0.72201	0.78287
C31	0.57678	0.7224	0.63625
C32	0.32088	0.77369	1.59724
C33	0.33509	0.73429	1.47203
C34	0.37433	0.73631	1.32839
C35	0.40403	0.77866	1.29019
C36	0.39015	0.81761	1.41583
C37	0.35136	0.81538	1.55885
N38	0.444	0.78542	1.13518
C39	0.46966	0.75574	1.01425

C40	0.51223	0.76344	0.85023
C41	0.77334	0.72761	-0.00171

Section 12. Supporting References

[S1] N. Fomina and T. E. Hogen-Esch, *Macromolecules*, 2008, **41**, 3765-3768.

[S2] Y.-B. Zhang, J. Su, H. Furukawa, Y. Yun, F. Gándara, A. Duong, X. Zou and O. M. Yaghi, *J. Am. Chem. Soc.*, 2013, **135**, 16336-16339.